

Anisotropic Permeability of Geomaterials: Lab Test and Borehole Environment Model



Larisa Nazarova , Nikita Golikov , Leonid Nazarov ,
and Galina Nesterova 

Abstract Theoretical substantiation and lab tests of the method for synthesis of a relationship describing angular anisotropy of the effective permeability in borehole environment based on the inverse coefficient problem solution in terms of the data on percolation tests of regularly non-uniform cylindrical specimens with a central hole are set forth in the paper. With a view to provide the algorithmic support of GIS data inversion in the course of determination of poroperm properties of production intervals the researchers developed and implemented by the hybrid numerical method to realize the multiphysical model of the evolution of geomechanical and electrohydrodynamic fields under filtration of multiphase fluid in the borehole environment with consideration for anisotropy of permeability induced by difference in components of the external stress fields. The numerical experiments enabled to establish that in the overbalanced drilling the configuration of invaded zone depends on the proportion between horizontal stress components outside of the well influence zone.

Keywords Mass transfer · Poroperm properties · Lab test · Anisotropic permeability · Pressure · Inverse problem

1 Introduction

To solve the problems on advance degassing of coal seams and coalmine methane utilization design (Seidle 2011), investigation of geothermal systems (Salimzadeh et al. 2018), construction of underground gas storages (Caglayan et al. 2020), inversion of geophysical borehole surveying data with the view to establish production intervals and to assess poroperm properties of rocks (Hsu and Robinson 2019; Ahmed 2019; Yeltsov et al. 2014; Garcia and Heidari 2021) and other actual problems

L. Nazarova (✉) · L. Nazarov
Chinakal Institute of Mining, Siberian Branch of the Russian Academy of Sciences, 54 Krasny Prospekt, 630091 Novosibirsk, Russia

N. Golikov · G. Nesterova
Trofimuk Institute of Petroleum Geology and Geophysics, Siberian Branch of the Russian Academy of Sciences, 3 Prospekt Koptyuga, 630090 Novosibirsk, Russia

requires the development of multiphysical models and their appropriate verification. Such models comprising the conservation law and state equations also involve empirical relationships between parameters of the physical field arising in borehole environment, such as petrophysical formulas of electroconductivity of a heterogenic medium, relationship of phase permeability versus fluid concentration, the reservoir rock poroperm properties—stress relationship. The last factor as well as probable difference between components of the external stress field and disturbance of rock mass stability caused by boring operations can provoke the permeability anisotropy in the vicinity of a borehole. Subsequently, the borehole environment can not be described in terms of one dimensional models (Yeltsov et al. 2012; Nazarova and Nazarov 2018), so 2D and 3D models should be used, but they imply the proper parametric base resting on respective experiments, where specific features of poroperm properties distribution are considered.

The paper reports the data on percolation tests of regularly heterogeneous cylindrical specimens with central hole. The specimens made of a synthetic geomaterial are used to work out a process for determination of the effective permeability—polar angle relationship based on solution of the inverse coefficient problem. The researchers propose 2D multiphysical model describing evolution of geomechanical and electrohydrodynamic fields in the borehole environment under multiphase filtration.

2 Anisotropic Permeability by Lab Test Data and Inverse Problem Solution

2.1 Experimental Design

Cylindrical specimens (height $h = 110$ mm, external radius $R = 75$ mm, central channel diameter $2a = 8$ mm) were assembled of six components of the same shape (Fig. 1a), but different permeability. The components were made of the conditioned cryogel consisted of three calibrated sand fractions (0.5, 1, and 1.5 mm) under the original technological process (Nazarova et al. 2019). Permeability values of specimen components assessed under the standard procedure (RF Standard 26450.2–85 1985), appeared $k_0 = 24$ mD, $k_1 = 29$ mD, and $k_2 = 35$ mD.

Specimen 1 in isolating rubber collar 2 was placed in sealed metal chamber 3 (Fig. 1b), the rest free space stuffed with coarse-grain sand 4 (fraction 5 mm) exhibited high permeability (more than 3 Darcy) and did not notably affect the filtration characteristics of the test system. The air was pumped under constant pressure p_m through central hole 5. The air flowrate Q_{mn} was recorded at a stationary mode with relative precision of 2% at side surface of the specimen segment (central angle $2\beta = 30^\circ$, Figs. 1a and 2), which position was determined by angle φ_n (the flowmeter was connected through adapter 6). Measurement results at $p_m = 1.05, 1.10, \dots, 1.25$ bar and $\varphi_n = 30^\circ, 45^\circ, \dots, 150^\circ$ are reported in Table 1.

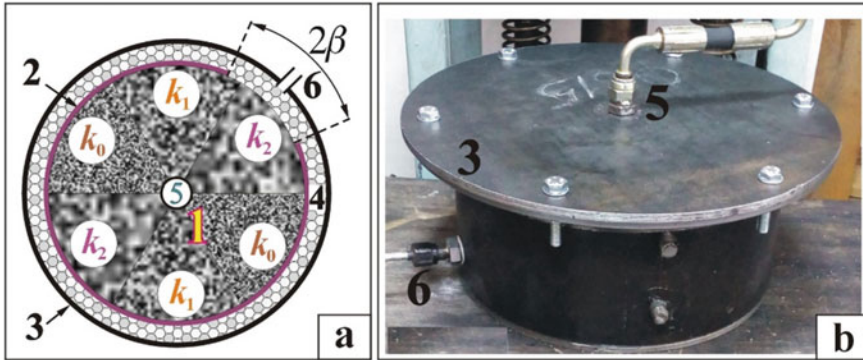


Fig. 1 Specimen structure (a) and test bench (b)

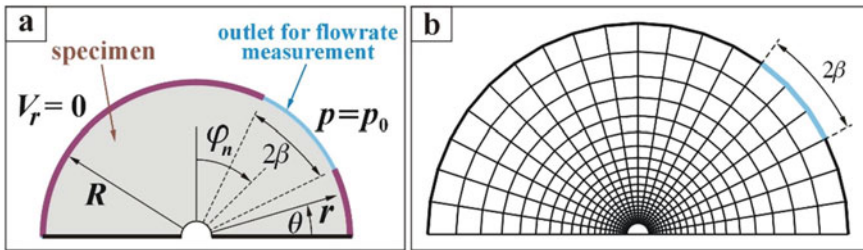


Fig. 2 Model of the experiment and boundary conditions (a), computational grid (b)

Table 1 Flowrate Q_{mn} (ml/min) at different input pressure p_m and angle φ_n

m	p_m (bar)	φ_n (deg)								
		30°	45°	60°	75°	90°	105°	120°	135°	150°
1	1.05	50	54	59	62	64	64	65	64	61
2	1.10	101	111	120	128	131	132	133	131	124
3	1.15	127	138	150	159	163	165	166	164	155
4	1.20	156	170	185	196	201	203	204	202	190
5	1.25	213	232	252	267	274	277	279	275	260

2.2 Model of the Percolation Experiment

Evolution of hydrodynamic fields in the test specimen in polar coordinates (r, θ) (Fig. 2a) is described by the system including (Kochin et al. 1964):

Continuity equation

$$\frac{\partial(\omega\rho)}{\partial t} + \operatorname{div}(\rho\vec{V}) = 0; \quad (1)$$

Darcy's law

$$\vec{V} = -\frac{K}{\eta} \operatorname{grad} p \quad (2)$$

and state equation

$$p = p_0\rho/\rho_0 \quad (3)$$

where ω —porosity, p —pressure, ρ and η —density and viscosity of gas, ρ_0 —gas density at atmospheric pressure p_0 , $\vec{V} = (V_r, V_\theta)$ —seepage velocity, permeability K is the piecewise constant function versus polar angle

$$K(\theta) = \begin{cases} k_0 & 0 \leq \theta \leq \pi/3, \pi \leq \theta \leq 4\pi/3 \\ k_1 & \pi/3 \leq \theta \leq 2\pi/3, 4\pi/3 \leq \theta \leq 5\pi/3 \\ k_2 & 2\pi/3 \leq \theta \leq \pi, 5\pi/3 \leq \theta \leq 2\pi \end{cases}$$

System (1)—(3) reduces to non-linear parabolic equation

$$\frac{\partial p}{\partial t} = b \operatorname{div}(Kp \operatorname{grad} p) \quad (4)$$

($b = \rho_0/\omega\eta p_0$) for which the following boundary conditions are formulated (Fig. 2a):

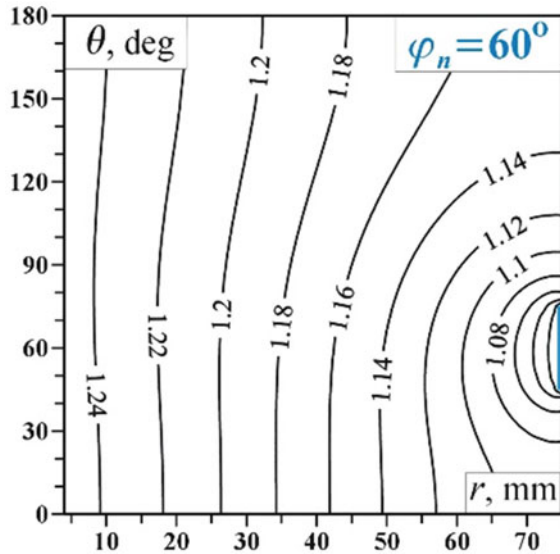
$$\begin{aligned} p(a, \theta, t) &= p_m; \\ (R, \theta, t) &= p_0 \quad \text{at} \quad |\theta - \varphi_n| \leq \beta; \\ V_r(R, \theta, t) &= 0 \quad \text{at} \quad |\theta - \varphi_n| > \beta. \end{aligned} \quad (5)$$

The flowrate through the sector at side surface of the specimen determined by angle φ_n (Figs. 1 and 2a) is calculated by formula

$$Q(t) = hR \int_{\varphi_n - \beta}^{\varphi_n + \beta} V_r(R, \theta, t) d\theta, \quad (6)$$

where radial velocity V_r is found from (2).

Fig. 3 Contour lines of p/p_0



System (4), (5) was solved by the finite-difference method of alternating directions (Samarskii 2001) at nonuniform grid (Fig. 2b). It is important to point out that stationary distribution of hydrodynamic field parameters does not depend on b value.

Pressure distribution (Fig. 3) in the specimen at the steady-state filtration mode at $\varphi_n = 60^\circ$ and $p_m = 1.25$ bar indicates the existence of depressed zones of comparatively low gradient far from the sector where the flowrate was measured.

2.3 Test Data Interpretation

The inverse problem statement runs as follows: using the measurement data on flow rates Q_{mn} (Table 1) it is required to find continuous function describing dependence of the effective permeability versus angle θ . Suppose that $K(\theta) = A + (B - A)\theta/\pi$ ($0 \leq \theta \leq \pi$) and introduce the objective function

$$\Psi(A, B) = \sqrt{45 \sum_{m=1}^5 \sum_{n=1}^9 [Q(A, B, p_m, t) - Q_{mn}]^2} / \sum_{m=1}^5 \sum_{n=1}^9 Q_{mn}$$

where Q —stationary flowrate, computed from (4), (6) at some A, B, p_m , and φ_n values. The minimum of function Ψ , which was determined by the modified conjugate-gradient method (Nazarov et al. 2013), provides solution of the inverse problem, viz., values of A and B coefficients.

Fig. 4 Level lines of objective function Ψ

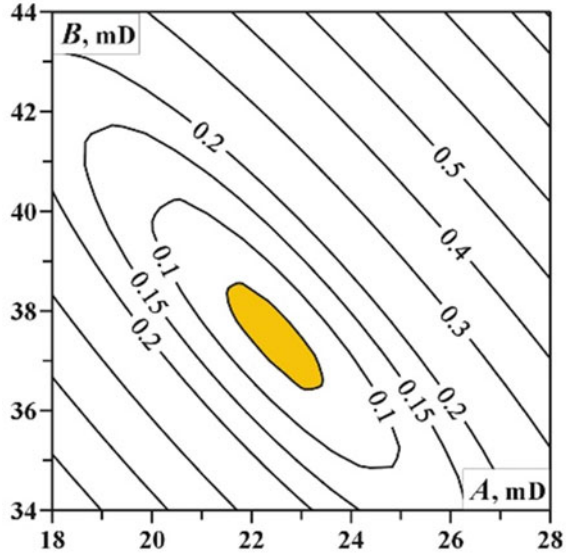


Figure 4 demonstrates level lines of the objective function, the toned area is equivalency domain $\Psi \leq 0.05$. It is obvious that Ψ is unimodal, so the stated inverse problem is uniquely solvable. Within up to 10% accuracy the target coefficients: $A = 22\text{--}23$ mD and $B = 37\text{--}38$ mD are in good compliance with permeability values k_0 , k_1 , and k_2 of separate sections of the test specimen.

3 Mass Transfer in Borehole Environment

Poroperm properties anisotropy is governed by both specific structural features of a seam and non-homogeneous stress state in well environment. Due consideration should be given to this peculiarity in modeling intended to describe mass transfer processes in the vicinity of borehole.

Let at time moment $t = 0$ a horizontal formation filled with a multiphase fluid and bounded with impermeable interfaces beds is penetrated to its entire thickness h by a vertical borehole of radius a . In the overbalanced drilling case when the initial reservoir pressure p_s is lower than bottom hole pressure p_b , a flashed zone and mud cake tend to come into being. The poroelastic model describing quasistatic deformation of a reservoir under two-phase fluid filtration includes:

Equilibrium equation

$$\sigma_{ij,j} = 0; \tag{7}$$

Hooke's law

$$\sigma_{ij} = \lambda \varepsilon_{ij} + 2\mu \varepsilon_{ij} - p \quad (8)$$

Cauchy's relations

$$\varepsilon_{ij} = 0.5(u_{i,j} + u_{j,i}) \quad (9)$$

continuity equation for each phase

$$\frac{\partial(\omega S_n)}{\partial t} + \text{div } \vec{V}_n = 0 \quad (10)$$

Darcy's law

$$\vec{V}_n = -\frac{K k_n}{\eta_n} \text{grad } p \quad (11)$$

salt transfer equation

$$\frac{\partial(\omega C S_1)}{\partial t} + \text{div}(C \vec{V}_1) = 0; \quad (12)$$

as well as empirical dependences of porosity ω versus pressure p

$$\omega = \omega_0 + \beta p; \quad (13)$$

permeability K versus effective stress (Nazarova and Nazarov 2018; Nazarova et al. 2019)

$$K = K_0 \exp(-\gamma \sigma_f) \quad (14)$$

and growth rate of mud cake thickness D versus flow rate Q (Yeltsov et al. 2012)

$$2\pi ah \frac{\partial D}{\partial t} = \psi Q, \quad (15)$$

where u_i , ε_{ij} , and σ_{ij} —components of displacement vector, strain and stress tensors; $i, j = r, \theta$; (r, θ) —cylindrical coordinates; δ_{ij} —Kronecker delta; λ, μ —Lame parameters; $\sigma_f = \sigma_{ii}/3 - p$; S_n —saturation of phase n (here $n = 1$ corresponds to drilling mud filtrate, $n = 2$ —oil, $S_1 + S_2 = 1$); C —salinity; $k_n = S_n^{\alpha_n}$ —relative phase permeability, α_n —empirical parameters; \vec{V}_n —seepage velocity; η_n —viscosity; β

and γ —fluid and reservoir rock compressibilities $\psi = \xi/(1 - \xi)(1 - \omega_m)$; ω_m —porosity of mud cake; ξ —clayey content in drill mud;

$$Q = ah \int_0^{2\pi} \left(\vec{V}_1(a, \theta, t) \right)_r d\theta.$$

System (7)–(15) is solved in domain $\{a \leq r \leq R, 0 \leq \theta \leq \pi\}$, with formulation of initial

$$p(r, \theta, 0) = p_s, \quad S_1(r, \theta, 0) = S_0, \quad C(r, \theta, 0) = C_0, \quad D(0) = 0 \quad (16)$$

and boundary

$$\begin{aligned} \sigma_{rr}(a, \theta) = p_b, \quad \sigma_{rr}(R, \theta) = (q_1 \cos^2 \theta + q_2 \sin^2 \theta) \sigma_V \\ \sigma_{r\theta}(a, \theta) = \sigma_{r\theta}(R, \theta) = 0 \end{aligned} \quad (17)$$

$$\begin{aligned} p(a, \theta, t) = p_b, \quad p(R, \theta, t) = p_b, \\ S_1(a, \theta, t) = S_m, \quad S_1(R, \theta, t) = S_0, \\ C(a, \theta, t) = C_m, \quad C(R, \theta, t) = C_m \end{aligned} \quad (18)$$

conditions (line $\theta = 0, \pi$ —symmetry axis), where R is size of well influence zone ($a \ll R$), S_0, C_0 —water saturation and salinity in an intact reservoir, S_m and C_m are water saturation and salinity of drill mud, q_1 and q_2 are lateral pressure coefficients corresponding to maximum σ_{\max} and minimum σ_{\min} horizontal stresses in the external field; $\sigma_V = \rho_1 g H$ is lithostatic stress at reservoir occurrence depth H , ρ_1 is average overlying rock density.

The stated boundary-value problem, implemented by the hybrid numerical method (Nazarova et al. 2020), enabled to develop the rapid computing algorithm at every time moment in the same grid (similar to grid in Fig. 2b); system (7)–(9) and (17) was solved by the finite element method (original code (Nazarova and Nazarov 2009)), while (10)–(16), (18) was solved by the finite-difference method of alternating directions) (Samarskii 2001).

Let exemplify the effect of “induced” anisotropy of permeability on distribution of electrohydrodynamic fields in borehole environment. The computation was based on the following model parameters matching to an actual production interval of an operating well, Kogalym oil deposit, West Siberia (Yeltsov et al. 2014): $H = 2518$ m, $\rho_1 = 2500$ kg/m³, $g = 9.81$ m/s², $\lambda = \mu = 20$ GPa, $a = 0.1$ m, $R = 2$ m, $K_0 = 34$ mD, $\eta_1 = 0.001$ Pa · s, $\eta_2 = 0.004$ Pa · s, $\alpha_1 = 2$, $\alpha_2 = 3$, $\beta = 10^{-9}$ 1/Pa, $\gamma = 10^{-10}$ 1/Pa, $\xi = 0.45$, $\omega_m = 0.2$, $q_1 = 0.7$, $q_2 = 0.62$, $p_s = (1 + q_1 + q_2) \sigma_V / 3$ (Khristianovich 1989), $p_b = 1.05 p_s$, $C_0 = 1$ g/l, $C_m = 20$ g/l, $S_0 = 0.3$, $S_m = 0.9$.

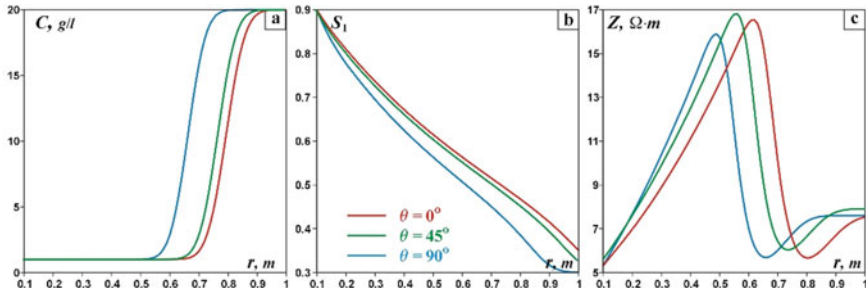


Fig. 5 Distribution of salinity C (a), water saturation S_1 (b) and true resistivity Z (c)

Figure 5 demonstrates distribution of water saturation S_1 , salinity C and true resistivity Z , calculated from Archie formula (Archie 1942) in modification (Yeltsov et al. 2012)

$$Z = \frac{A}{\omega^2 C (S_0 + S_1)^2},$$

(A —empiric constant) at time moment $t = 2$ days. It is obvious that minor difference between horizontal stress components in the external field leads to qualitative alteration in distribution of information-bearing parameters applicable to inverse logging data. In particular, drill mud penetration values in direction of σ_{max} action are 15–20% higher than similar magnitudes in orthogonal direction.

This factor should be taken into account to inverse the evidence obtained by advanced borehole geoelectrical methods (Yeltsov et al. 2014; Garcia et al. 2019; Bennis and Torres-Verdin 2019).

Acknowledgements The work was carried out with partial financial support of the Russian Foundation for Basic Research (Project No. 19-05-00689) and Programs of Federal Scientific Investigations: Identification Numbers AAAA-A17-117122090002-5 and 0331-2019-0015.

References

Ahmed TH (2019) Reservoir engineering handbook, 5th edn. Gulf Professional Publishing, Oxford
 Archie GE (1942) The electrical resistivity log as an aid in determining some reservoir characteristics. Trans AIME 146:54–62
 Bennis M, Torres-Verdin C (2019) Estimation of dynamic petrophysical properties from multiple well logs using machine learning and unsupervised rock classification. In: SPWLA 60th annual logging symposium, the Woodlands, Texas, USA. Expanded abstract: paper number: SPWLA-2019-KKKK
 Caglayan D, Weber N, Heinrichs HU, Linßen J, Robinius M, Kukla PA, Stolten D (2020) Technical potential of salt caverns for hydrogen storage in Europe. Int J Hydrogen Energy 45:6793–6805

- Garcia AP, Heidari Z (2021) A new multiphysics method for simultaneous assessment of permeability and saturation-dependent capillary pressure in hydrocarbon-bearing rocks. *SPE J* 26(1):155–171
- Garcia P, Heidari Z, Torres-Verdin C (2019) Multi-frequency interpretation of electric resistivity and dielectric permittivity measurements for simultaneous assessment of porosity, water saturation, and wettability (expanded abstract) In: SPWLA 60th annual logging symposium, the Woodlands, Texas, USA. Paper number: SPWLA-2019-III
- Hsu CS, Robinson PR (2019) *Petroleum science and technology*. Springer, New York
- Khrisianovich SA (1989) *Fundamentals of seepage theory*. *Sov Min Sci* 25:397–412
- Kochin NE, Kibel IA, Roze NV (1964) *Theoretical hydromechanics*. Wiley, Chichester
- Nazarov LA, Nazarova LA, Karchevskii AL, Panov AV (2013) Estimation of stresses and deformation properties in rock mass based on inverse problem solution using measurement data of free boundary displacement. *J Appl Ind Math* 7(2):234–240
- Nazarova LA, Nazarov LA (2009) Dilatancy and the formation and evolution of disintegration zones in the vicinity of heterogeneities in a rock mass. *J Mining Sci* 45(5):411–419
- Nazarova LA, Nazarov LA (2018) Geomechanical and hydrodynamic fields in producing formation in the vicinity of well with regard to rock mass permeability-effective stress relationship. *J Mining Sci* 54(4):541–549
- Nazarova LA, Nazarov LA, Skulkin AA, Golikov NA (2019) Stress-permeability dependence in geomaterials from laboratory testing of cylindrical specimens with central hole. *J Mining Sci* 55(5):708–714
- Nazarova LA, Skulkin AA, Golikov NA, Nazarov LA (2020) Experimental investigation of poroperm properties of geomaterials in non-uniform stress field. *J Mining Sci* 56(5):706–712
- RF Standard 26450.2–85 (1985) *Rocks. Method for determination of absolute gas permeability coefficient by stationary and non-stationary filtration*
- Salimzadeh S, Paluszny A, Nick HM, Zimmerman RW (2018) A three-dimensional coupled thermo-hydro-mechanical model for deformable fractured geothermal systems. *Geothermics* 71:212–224
- Samarskii AA (2001) *The theory of difference schemes*. Marcel Dekker Inc., New York
- Seidle J (2011) *Fundamentals of coalbed methane reservoir engineering*. PennWell Books, Tulsa
- Yeltsov IN, Nesterova GV, Kashevarov AA (2012) Invasion zone modeling using water- and oil-based muds. *J Appl Mech Technical Phys* 53(4):552–558
- Yeltsov IN, Nesterova GV, Sobolev AY, Epov MI, Nazarova LA, Nazarov LA (2014) Geomechanics and fluid flow effects on electric well logs: multiphysics modeling. *Russ Geol Geophys* 55(5–6):775–783